Exocyclically metallated tetrapyridinoporphyrazine as a potential photosensitizer for photodynamic therapy

Schneider, Lukas ; Larocca, Michele ; Wu, Wenyu ; Babu, Vipin ; Padrutt, Roxane ; Slyshkina, Ekaterina ; König, Christiane ; Ferrari, Stefano ; Spingler, Bernhard

Abstract: We report the first exocyclically metallated tetrapyridinoporphyrazine, [tetrakis-(trans-Pt(NH3)2Cl)-tetra(3,4-pyrido)porphyrazine-zinc(II)](NO3)4 (4), synthesized in a multistep synthesis starting from 3,4-pyridinedicarbonitrile (1). The synthetic procedure involved a platination reaction of the intermediate tetra(3,4-pyrido)porphyrazine-zinc(II) (2), whereby the zinc(II) enhanced the solubility of the intermediate enabling the platination reaction. A similar approach to synthesize [tetrakis-(trans-Pt(NH3)2Cl)-tetra(3,4-pyrido)porphyrazine](NO3)4 (5) failed due to the unsuitable solubility properties of the intermediate tetra(3,4-pyrido)porphyrazine (3). The final product 4 and the intermediates were characterized, the photochemical and photophysical properties were determined and the photocytotoxicities were investigated. We demonstrate that the platinated tetra-pyridinoporphyrazine 4 is a potential photosensitizer for photodynamic therapy (PDT).

DOI: https://doi.org/10.1039/c9pp00336c

Photochemical & Photobiological Sciences

PAPER

Cite this: *Photochem. Photobiol. Sci.*, 2019, **18**, 2792

Exocyclically metallated tetrapyridinoporphyrazine as a potential photosensitizer for photodynamic therapy†

Lukas Schneider, [a] Michele Larocca, [a] Wenyu Wu,[a] Vipin Babu, [a] Roxane Padrutt, [a] Ekaterina Slyshkina, [a] Christiane König,[b] Stefano Ferrari *[b,c] and Bernhard Spingler *[a]

Received 12th August 2019,
Accepted 11th October 2019

DOI: 10.1039/c9pp00336c

rsc.li/pps

We report the first exocyclically metallated tetrapyridinoporphyrazine, [tetrakis-(*trans*-Pt$(NH_3)_2$Cl)-tetra(3,4-pyrido)porphyrazine-zinc(II)]$(NO_3)_4$ (**4**), synthesized in a multistep synthesis starting from 3,4-pyridinedicarbonitrile (**1**). The synthetic procedure involved a platination reaction of the intermediate tetra(3,4-pyrido)porphyrazine-zinc(II) (**2**), whereby the zinc(II) enhanced the solubility of the intermediate enabling the platination reaction. A similar approach to synthesize [tetrakis-(*trans*-Pt$(NH_3)_2$Cl)-tetra(3,4-pyrido)porphyrazine]$(NO_3)_4$ (**5**) failed due to the unsuitable solubility properties of the intermediate tetra(3,4-pyrido)porphyrazine (**3**). The final product **4** and the intermediates were characterized, the photochemical and photophysical properties were determined and the photocytotoxicities were investigated. We demonstrate that the platinated tetra-pyridinoporphyrazine **4** is a potential photosensitizer for photodynamic therapy (PDT).

Introduction

Photodynamic therapy (PDT) is a powerful therapeutic method that utilizes a photosensitizer (PS), activated by light, to create irreversible damage to the target tissue. PDT is widely used for the treatment of a variety of premalignant and malignant diseases.[1–8] Besides being a valuable therapy in oncology, it is applied as a treatment for localized infections, arterial diseases and menorrhagia.[9] The non-invasive nature of the treatment together with the possibility for spatial and temporal control, lack of cumulative toxicity and compatibility with other treatment methods render PDT a very attractive therapeutic method for different types of cancer.[2,9]

PDT uses three main components; a PS, light of a specific wavelength, and molecular oxygen in the tissue. The PS is introduced into the organism where it accumulates in the tissue to be treated. Further, the tissue-localized PS is excited from its singlet ground state (S_0) to the first excited state (S_1) by light of an adequate wavelength. After undergoing intersystem crossing (ISC) from the S_1 state, the energetically lower long-lived triplet state (T_1) of the PS can generate singlet oxygen ($^1O_2$) and/or other reactive oxygen species (ROS) while the PS relaxes to its ground state.[10] The generated ROS cause cellular damage leading to the induction of cell death pathways.[1,4]

An ideal PS should exhibit a high chemical stability, low dark toxicity, specificity to the target tissue as well as strong electronic transition intensities between 650 nm and 850 nm, referred to as the *phototherapeutic window*.[11] Wavelengths shorter than 650 nm display low tissue penetration and wavelengths longer than 850 nm are unable to induce the ROS-creating PS pathways due to a lack of energy.[9] Additionally, the PS requires amphiphilic properties for the transportation inside the body and cellular uptake.[3,11] Current PDT limitations are mostly attributed to PSs with absorption ranges below 650 nm, resulting in a low tissue penetration of the required light. Furthermore, *in vivo* accumulation of PSs due to hydrophobic interactions results in a reduced cellular uptake, lowering the efficiency of the treatment.[12,13]

Our group has previously reported the synthesis of exocyclically tetraplatinated porphyrins.[14] These compounds displayed high phototoxic indexes (PI) against cancer cells, high singlet oxygen quantum yields (Φ_Δ) and a relevant cellular uptake.[14] However, porphyrins are known to exhibit twenty times higher excitation coefficients in the blue region of the electromagnetic spectrum compared to the red region that lies in the *phototherapeutic window*.[8,11,15] To counter these PDT limit-

[a]*Department of Chemistry, University of Zurich, Winterthurerstrasse 190, 8057 Zurich, Switzerland. E-mail: spingler@chem.uzh.ch; Fax: +4144 635 68 02; Tel: +41 44 635 46 56; http://www.chem.uzh.ch/en/research/groups/spingler.html*
[b]*Institute of Molecular Cancer Research, University of Zurich, Winterthurerstrasse 190, 8057 Zurich, Switzerland. E-mail: sferrari@imcr.uzh.ch; Fax: +4144 635 34 84; Tel: +41 44 635 34 71; http://www.imcr.uzh.ch/research/Alumni-Ferrari.html*
[c]*Institute of Molecular Genetics of the Czech Academy of Sciences, Videnska 1083, 143 00 Prague, Czech Republic*

†Electronic supplementary information (ESI) available. See DOI: 10.1039/c9pp00336c

ations of porphyrins, we propose the investigation of exocyclically platinated tetra(pyrido)porphyrazine-based PSs. Tetra(pyrido)porphyrazines and phthalocyanines are planar aromatic macrocycles related to porphyrins and they display an exceptional stability as well as a strong light absorption around 670 nm, rendering them ideal for PDT in terms of absorption properties.[10]

In order to counter their high aggregation tendency and low solubility in aqueous media, we propose the exocyclic platination of tetra(pyrido)porphyrazines which induces a fourfold positively charged character. The exocyclic platination constitutes an alternative to the incorporation of hydrophilic side groups.[1] Cationic porphyrazines were previously reported to exert an antibacterial effect and Zimcik and co-workers have reported a twelvefold cationic tetra(pyrido)porphyrazine, which displays an excellent dark to light toxicity ratio.[16,17] Additionally, various pyridyl-substituted porphyrazines, which were coordinated to palladium or platinum, are reported in literature.[18–21] However, to the best of our knowledge, no exocyclically metallated tetra(pyrido)porphyrazines have been reported so far.

Cisplatin is a known and extensively used chemotherapeutic drug for the treatment of different cancer types including ovarian and testicular cancer, whereby it induces cytotoxicity by interfering with the DNA replication.[14,22] Hence, in addition to improving the PDT efficiency, the exocyclic platination of tetra(pyrido)porphyrazines can render the compound a potential dual chemotherapeutic agent.[14] Upon intravenous administration, cisplatin maintains a relatively stable neutral state and forms cationic aqua complexes after cellular uptake due to the lower intracellular chloride concentration. These positively charged aqua complexes are unable to diffuse out of the cell and bind to intracellular targets, most notably DNA, which constitutes the main target.[23] Therefore, the platination of PSs could lead to a higher accumulation of the PS in cancerous cells, resulting in a more efficient treatment. Current clinically used platinum(II) drugs show side effects such as nephrotoxicity, ototoxicity, hepatotoxicity and cardiotoxicity. Moreover, they are ineffective against certain cancer types due to intrinsic or acquired resistance and these limitations call for new improved platinum(II)-based chemotherapeutic agents.[14,24]

In our previous study, a porphyrin coupled to transplatin showed the highest efficiency.[14] Similarly, we reacted tetra(3,4-pyrido)porphyrazines with four equivalents of transplatin, resulting in the synthesis of [tetrakis-(*trans*-$Pt(NH_3)_2Cl$)-tetra(3,4-pyrido)porphyrazine-zinc(II)]$(NO_3)_4$ (**4**). The compound was characterized for its photochemical and photophysical properties along with photocytotoxicity, DNA-binding constant and intracellular localization in HeLa cells.

Results and discussion

Synthetic procedures

The syntheses of two tetra(3,4-pyrido)porphyrazines were executed with 3,4-pyridinedicarbonitrile (**1**) as starting material, resulting in tetra(3,4-pyrido)porphyrazine-zinc(II) (**2**)[25–27] and 29*H*,31*H*-tetra(3,4-pyrido)porphyrazine (**3**).[28] Both syntheses were carried out according to literature reports, **2** as reported by Dupouy *et al.*[27] and **3** was synthesized according to the procedure reported by Ramirez *et al.*[28] (Scheme 1).

Both tetra(3,4-pyrido)porphyrazines were synthesized in a one-step synthesis, with DBU acting as base, catalyzing the reactions. The main difference is the presence of $Zn(OAc)_2{\cdot}2H_2O$ in the synthesis of **2**, resulting in zinc(II) acting as a template to facilitate the cyclotetramerization, which is reflected in the in the high yield of 64%. During the formation of **3** however, the lack of a metal ion lead to the formation of various polymers. This resulted in a lower yield of **3** (28%) compared to **2**.

During the reaction, DBU deprotonates the alcohol which then undertakes a nucleophilic attack on both the nitrile groups, leading to two different intermediates. Hence, the cyclotetramerization process leads to four different regioisomers of **2** and **3** (Fig. 1).

A reaction mechanism for the synthesis of phthalocyanines from phthalonitriles was proposed by Tomoda *et al.*[29] This mechanism is equivalent to the synthesis of the tetra(3,4-pyrido)porphyrazines reported in this work and is shown in the ESI (Scheme S1†).

The presence of **2** and **3** was confirmed with IR and UV-Vis spectroscopy as well as with (+)-ESI-MS and EA. Due to the low solubility emerging from the large conjugated aromatic systems of both tetra(3,4-pyrido)porphyrazines, **2** and **3** could not be characterized by ^{1}H-NMR and ^{13}C-NMR spectroscopy. This is a known limitation, as no NMR data were reported for both **2** and **3** in literature so far.[25–28] Characterization of **2** by ^{1}H-NMR spectroscopy was reported by Szulbinski *et al.*,[25] however, the corresponding data could not be found in the publication.

In a second step, **2** and **3** were further used to synthesize the two tetraplatinated compounds [tetrakis-(*trans*-$Pt(NH_3)_2Cl$)-tetra(3,4-pyrido)porphyrazine-zinc(II)]$(NO_3)_4$ (**4**) and [tetrakis-(*trans*-$Pt(NH_3)_2Cl$)-tetra(3,4-pyrido)porphyrazine]$(NO_3)_4$ (**5**). Transplatin (**6**) was used for both reactions and was pre-activated with $AgNO_3$ in DMF according to our previously reported procedure.[14] The formed [*trans*-$Pt(NH_3)_2Cl]NO_3$ (**7**) was then used for the tetraplatination of both tetra(3,4-pyrido)porphyrazines **2** and **3** (Scheme 2).

The platination approach with DMF as solvent was successful in the case of **4** with a yield of 48%. The same platination approach failed in the case of **5** due to the low solubility of **3**. A further approach involving the use of an EtOH/DMF mixture as solvent for the tetraplatination of **3** was similarly unsuccessful. This indicates that in contrast to the tetraplatinated 5,10,15,20-tetra(4-pyridyl)porphyrin compounds[14] reported previously by our group, free base tetra(3,4-pyrido)porphyrazines exhibit a too low solubility to be used for platination reactions. Therefore, we propose the investigation of exocyclically tetraplatinated metallo-tetra(pyrido)porphyrazines as potential PSs for PDT, as the presence of zinc(II) enhanced the solubility and enabled a exocyclic platination

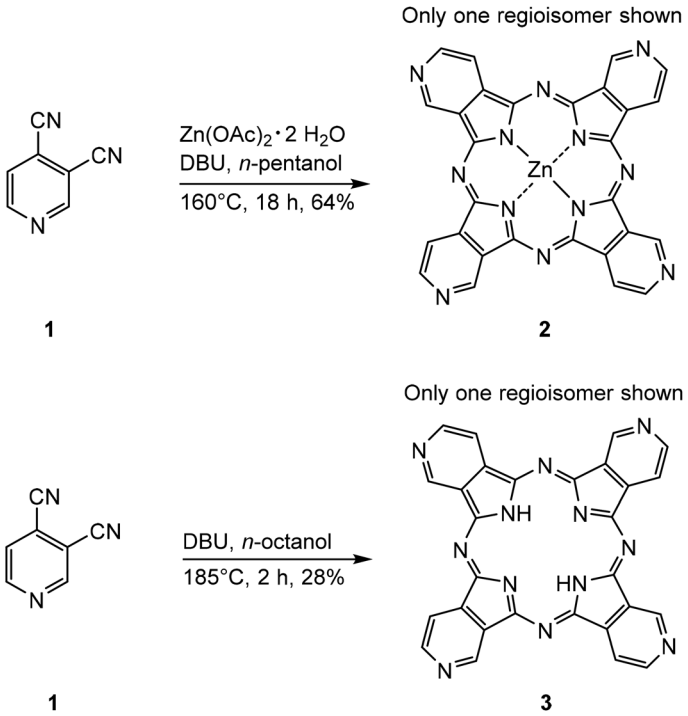

Scheme 1 Syntheses of tetra(3,4-pyrido)porphyrazine-zinc(II) (**2**) and 29*H*,31*H*-tetra(3,4-pyrido)porphyrazine (**3**).[27,28]

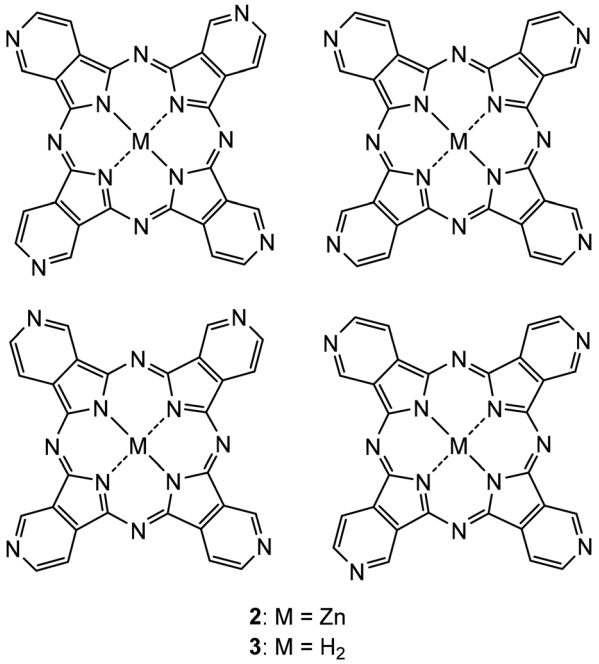

Fig. 1 The four regioisomers formed during the syntheses of **2** and **3**.

of **2** compared to its free base analogue **3**. The presence of **4** could be verified by IR, UV-Vis and ^{195}Pt-NMR spectroscopy as well as by (+)-ESI-MS and EA. The (+)-ESI-MS and ^{195}Pt-NMR spectrum clearly indicate the formation of **4** as the only platinated species. The ^{195}Pt-NMR spectrum of **4** is shown in the ESI (Fig. S1†).

Photochemical and photophysical properties

UV-Vis absorbance spectra of both the non-platinated tetra(3,4-pyrido)porphyrazines **2** and **3** as well as the tetraplatinated compound **4** were measured in DMF. The comparison of the absorbance spectra of **2** and **3** shows a similar absorption spectrum with two Q-bands at 663 and 674 nm in the case of **2** and at 660 and 669 nm for **3**, respectively. Also, the B-band is similarly located at 380 nm in the case of **2** compared to 388 nm in the case of **3**. The absorbance spectrum of **4** shows that the platination redshifts both the B-band and Q-bands, leading to a B-band at 402 nm and two Q-bands at 680 and 692 nm in the case of **4**. The superimposed UV-Vis spectra of **2**, **3** and **4** are shown in Fig. 2.

Fluorescence emission spectra of **2**, **3** and **4** were measured in DMF. The superimposed normalized fluorescence emission spectra are shown in Fig. 3. All three tetra(3,4-pyrido)porphyrazines were excited at 640 nm. The fluorescence emission maxima of the three compounds are similar showing values of 680 nm, 678 nm, 678 nm for **2**, **3** and **4**, respectively. Compared to the UV-Vis absorption spectra, a red-shift is observed in the case of the non-platinated tetra(3,4-pyrido)porphyrazines **2** and **3** and a small blue-shift was observed in the case of **4**.

Fluorescence emission lifetimes (τ) of **2**, **3** and **4** were measured as solutions in DMF with a 640 nm excitation wavelength (Table 1). All three samples **2**, **3** and **4** showed similar τ around 3.00 ns (τ = 3.06 ns for **2**, 2.99 ns for **3** and 2.80 ns for **4**). These values suggest that metallotetrapyridinoporphyrazines and free base tetrapyridinoporphyrazines do not differ in fluorescence emission lifetimes and that the exocyclic platina-

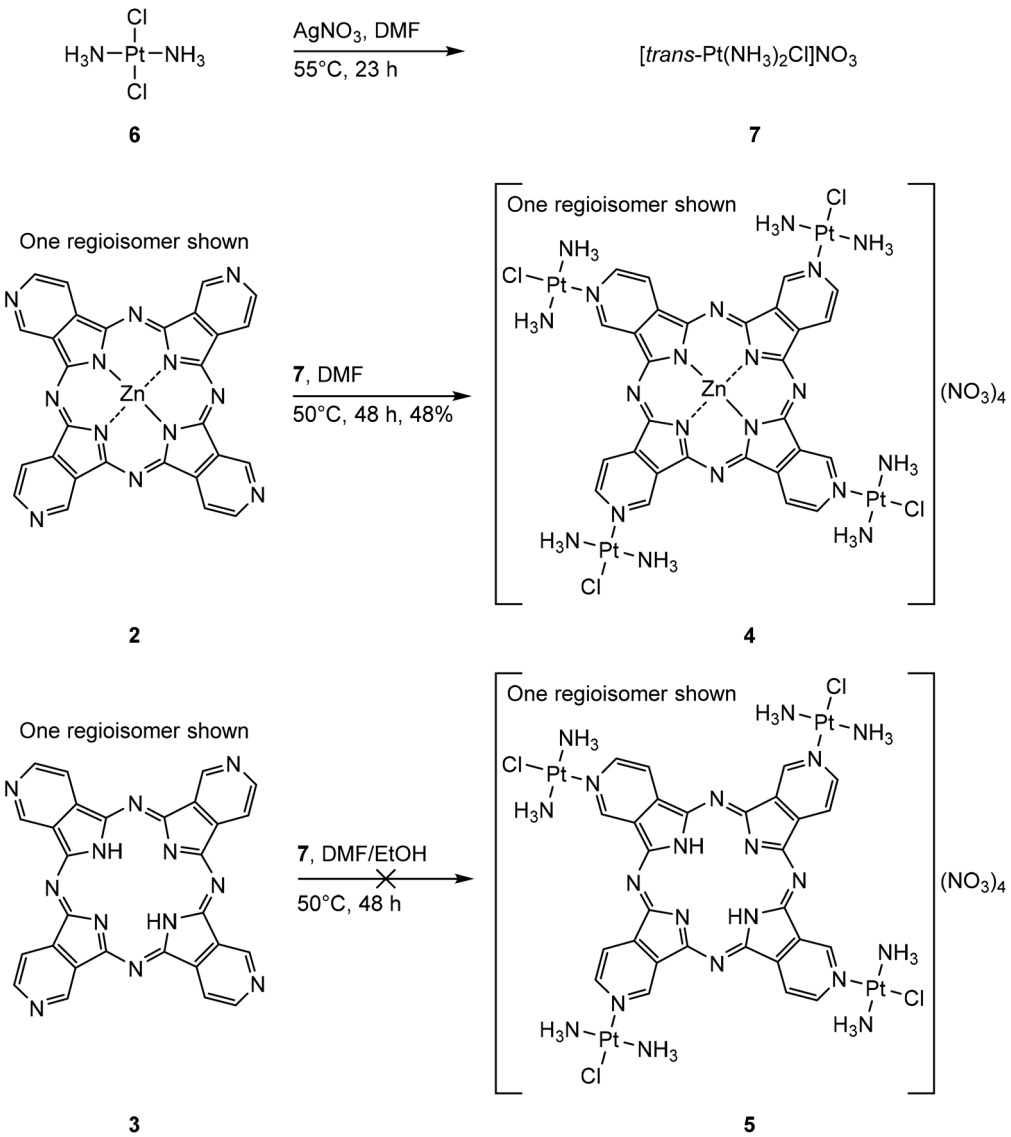

Scheme 2 Synthetic procedure for the synthesis of [tetrakis-(*trans*-$Pt(NH_3)_2Cl$)-tetra(3,4-pyrido)porphyrazine-zinc(II)]$(NO_3)_4$ (**4**) and the attempted synthesis of [tetrakis-(*trans*-$Pt(NH_3)_2Cl$)-tetra(3,4-pyrido)porphyrazine]$(NO_3)_4$ (**5**).

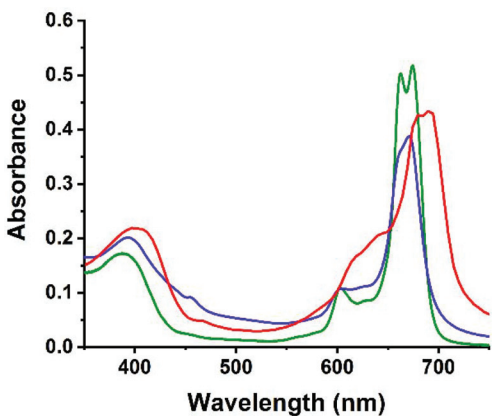

Fig. 2 UV-Vis absorbance spectra for **2** (green), **3** (blue) and **4** (red) (c = 6.0×10^{-5} M) measured in DMF.

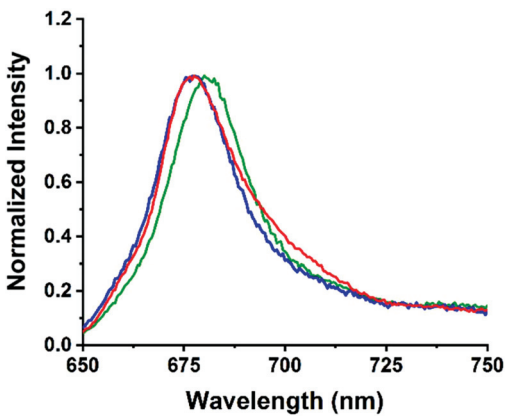

Fig. 3 Normalized fluorescence emission spectra of **2** (green), **3** (blue) and **4** (red) measured in DMF with a 640 nm excitation wavelength.

Table 1 Photochemical and photophysical parameters of **2**, **3** and **4** measured in DMF respectively DMF-d_7 in the case of Φ_Δ values

Substance	2	3	4
B-Band ($\lambda_{ab.}$)	380 nm	388 nm	402 nm
Q-Bands ($\lambda_{ab.}$)	663/674 nm	660/669 nm	680/692 nm
Fluorescence ($\lambda_{ex.}$ = 640 nm)	680 nm	678 nm	678 nm
τ [ns] ($\lambda_{ex.}$ = 640 nm)	3.06	2.99	2.80
Φ_f ($\lambda_{ex.}$ = 640 nm)	0.15 ± 0.02	0.07 ± 0.02	0.01 ± 0.02
Φ_Δ	0.21 ± 0.02	0.06 ± 0.01	0

tion does not shorten the lifetime of metallotetrapyridinoporphyrazines considerably.

Fluorescence quantum yields (Φ_f) of **2**, **3** and **4** were measured in DMF with an excitation wavelength of 640 nm (Table 1). The determined Φ_f values were 0.15 ± 0.02 for **2**, 0.07 ± 0.02 for **3** and 0.01 ± 0.02 for **4**. A major difference was observed for the Φ_f of **4** and its non-platinated precursor **2**, with **2** showing a Φ_f 14-times larger than **4**. This difference is attributed to the attached platinum nuclei in the case of **4**. Platinum(II) is reported to induce a heavy atom effect when attached to the photochemical system of a PS leading to larger percentages of ISC and hence, a smaller percentage of relaxation through fluorescence emission.[30,31] This behavior is desired in the case of PSs for PDT as a higher rate of ISC and relaxation through ROS production renders a PS more efficient. This underlines an additional beneficial property of platinated PSs for PDT, next to the improved solubility in aqueous media, improved cellular uptake and potential dual chemotherapeutic effect.

The singlet oxygen quantum yields (Φ_Δ) of **2**, **3** and **4** were determined based on the phosphorescence of the emerging singlet oxygen ($^1O_2$) at 1270 nm (Table 1). All three compounds were dissolved in DMF-d_7 and excited at 630 nm, as deuterated solvents were reported to increase the $^1O_2$ lifetime, leading to a more precise determination of the Φ_Δ values.[32] Φ_Δ values of 0.21 ± 0.02 and 0.06 ± 0.01 were obtained for **2** and **3**, respectively, which is in line with the Φ_f results, as the aggregation of **3** in DMF is higher compared to **2**, leading to smaller quantum yield values. The low Φ_Δ prevents **3** from being an efficient PS, meanwhile the Φ_Δ of **2** justifies further optimization through platination. Interestingly, no phosphorescence at 1270 nm from generated $^1O_2$ was observed in the case of compound **4**. This indicates that the tetraplatination has an effect on the type of ROS species produced by the PS, as the non-platinated precursor **2** was able to produce $^1O_2$ in contrast to **4**. To verify that **4** undergoes another mechanism upon irradiation leading to the production of other ROS species such as hydroxyl radicals that do not exhibit phosphorescent properties at 1270 nm, intracellular ROS production experiments were performed with **4**.

Photostability experiments of **2**, **3** and **4** were measured in DMF. The solutions used for the UV-Vis data were remeasured after one week under light exclusion and for a second time after an additional week in day light. In both measurements, no significant decay was observed, indicating that **2**, **3** and **4** are photostable in solution (Fig. S2†).

Photocytotoxicity experiments

In vitro photocytotoxicity assays were carried out to evaluate the anti-cancer activity of **2** and **4** (Fig. 4). As the nucleus regulates gene expression and controls replication during cell cycle, (light-induced) DNA damage caused by the PS inhibits the cell division in cancer cells, leading to one of the various cell death pathways.[1,4] IC_{50} values of **2** and **4** were determined in the HeLa cell line in the dark as well as after irradiation with light to investigate the photocytotoxicity of **2** and **4**. The IC_{50} values of **2** turned out to be relatively high (34 μM in the dark and 28 μM after irradiation with light), resulting in a phototoxic index (PI) of 0.8, which indicates that compound **2** lacks a significant photocytotoxicity. Conversely, **4** showed a lower IC_{50} value not only after light irradiation but also in the dark (12 μM in the dark and 1.6 μM after irradiation with light), resulting in a PI of 7.5. These results show, that **4** acts as a dual chemotherapeutic agent, as the dark toxicity IC_{50} value of **4** is almost three times lower compared to **2** due to the DNA-binding ability of the attached platinum complexes, inducing at the same time a photocytotoxicity that was not observed in the case of compound **2**. A comparison experiment with the well-known chemotherapeutic drug cisplatin (**CisPt**) showed that **CisPt** exhibits an even higher IC_{50} value (17.9 μM) under light exclusion compared to **4**, while not showing any photocytotoxicity after irradiation with light as expected (17.4 μM). These results underline the dual chemotherapeutic effect of **4** and show that single digit micromolar concentrations of **4** are able to induce photocytotoxicity.

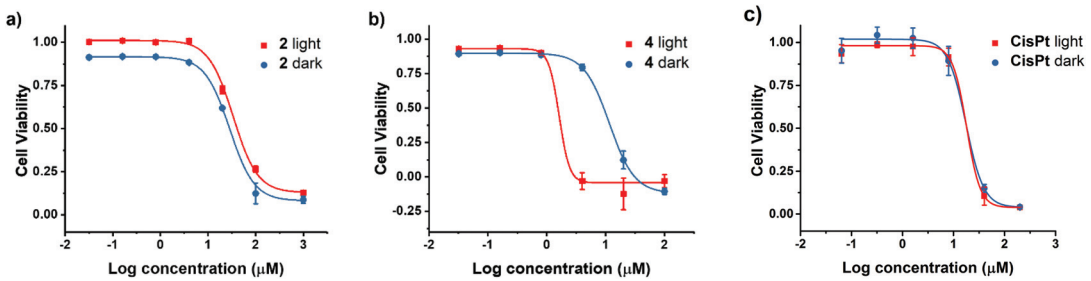

Fig. 4 Results of dose-dependent cell viability assays of **2** (a), **4** (b) and **CisPt** (c) in HeLa cells. Cells were incubated with either **2**, **4** or **CisPt** for 4 h and subsequently treated with red light for 20 min. Cell viability was determined using resazurin after 72 h.

Table 2 A comparison of phototoxic indices (PI) of porphyrazine compounds reported in literature

Cpd.	Cell line	Dark toxicity	Light toxicity	Light source	PI	Ref.
Pz-PB	A431	>60 μM	20 μM	LED, λ 615–635 nm, 10 J cm^{-2}	>3	36
Zn10	HeLa	105 μM	0.26 μM	Xe lamp, λ > 570 nm, 11 J cm^{-2}	404	33
2	HeLa	34 μM	28 μM	Halogen lamp, λ > 600 nm, 6.96 J cm^{-2}	0.8	This work
4	HeLa	12 μM	1.6 μM	Halogen lamp, λ > 600 nm, 6.96 J cm^{-2}	7.5	This work
Pz1	HSC-3	>10 μM	0.13 μM	LED, λ 690 nm, 3.6 J cm^{-2}	>77	34
Pc 5	HSC-3	>10 μM	0.022 μM	LED, λ 690 nm, 3.6 J cm^{-2}	>455	35

A comparison of the PI values of both tetrapyridinoporphyrazines **2** and **4** with other porphyrazines reported in literature is shown in Table 2. The selection of compounds was based on the usage of similar light intensities for the determination of the PI values. The comparison shows that **2** is indeed not applicable as a potential photosensitizer for PDT, as it lacks photocytotoxicity. On the contrary compound **4** shows photocytotoxicity, however the PI value is rather small compared to other porphyrazines reported in literature.[33–35] This is attributed to the low dark toxicity value of **4**, as none of the compared porphyrazines was designed to cause a dual chemotherapeutic effect. Therefore, the PI value of **4** is not directly comparable with the values reported for these porphyrazines.

The intracellular localization of **4** was investigated using fluorescence microscopy (Fig. 5 and S3†). HeLa cells were treated with **4** (50 μM, red), stained with Hoechst 33258 (blue, showing the nucleus) and imaged using high resolution confocal laser scanning microscopy (CLSM). The results show that **4** is taken up by the cancer cells from the extracellular environment within 2 h. Compound **4** mainly accumulates in the nucleus, suggesting that **4** interacts with DNA, leading to subsequent DNA damage and resulting in photocytotoxicity. Additionally, no staining of the cytoplasmic or nuclear membranes by compound **4** was detected.

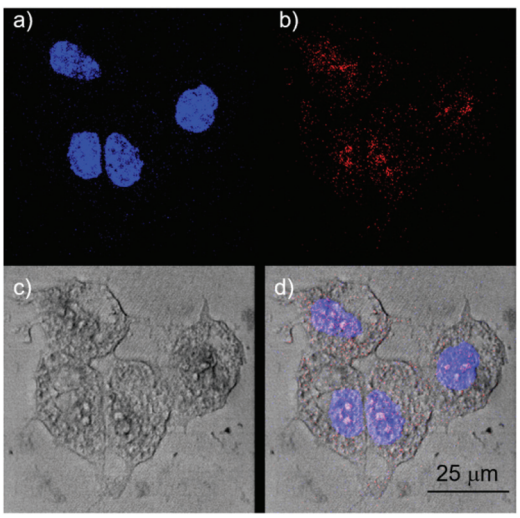

Fig. 5 The intracellular localization of compound **4** in HeLa cells. Cells were incubated with compound **4** for 2 h prior to imaging. Confocal images of cells doubly stained with Hoechst 33258 (a), **4** (b), wide-field (c) and merged images (d) are presented.

The DNA-binding ability of **4** was determined with an ethidium bromide (EB) intercalator displacement assay (Fig. 6). The competition of **4** with EB for intercalating sites on ctDNA was investigated by fluorescence emission during an EB displacement titration. The competitive binding of **4** was calculated as the apparent binding constant K_{app} using fluorescence spectra of EB (2 μM) saturated with ctDNA (100 μM) in a 9 : 1 PBS/DMF solvent mixture similar to our previous publication[14] using eqn (E1) reported by Boger *et al.*[37]

$$K_{app} = K_{EB}\frac{[EB]}{[4]}. \quad \text{(E1)}$$

In (E1), K_{EB} is the binding constant for EB (K_{EB} = 1.0 × 10^7 M^{-1}), [EB] designates the concentration of EB (2 μM) and [**4**] designates the concentration of **4** at 50% quenching of the ctDNA bound EB fluorescence emission.

The fluorescence emission of the intercalated EB at 600 nm (λ_{ex} = 546 nm) was monitored with stepwise increase in concentration of **4**, whereby the fluorescence emission intensity of the intercalated EB spectrum decreased as a result of the competitive intercalating of **4** in ctDNA. A quenching of 50% of the ctDNA bound EB fluorescence emission was observed at a photosensitizer concentration of 13.8 μM, resulting in a K_{app} of 1.4 × 10^6 M^{-1}. This binding constant shows a weaker intercalation activity for ctDNA compared to EB while neglecting the crosslinking activity of **4** that is not present in EB.

Further, we investigated whether the phototoxicity exhibited by **4** could be attributed to increased intracellular ROS levels (Fig. 7 and S4†). HeLa cells were treated with 12 μM of **4** and subjected to irradiation by the same light as used for the photocytotoxicity assays. The ROS levels were detected using 2′,7′-dichlorodihydrofluorescein diacetate (H_2DCF-DA) followed by fluorescence-activated cell sorting (FACS) analysis. The non-fluorescent H_2DCF-DA is converted into fluorescent 2′,7′-dichlorohydrofluorescein (DCF) upon oxidation by intracellular ROS produced by photoactivation of the PS.[5,38] Cells treated with **4**, displayed significantly higher ROS levels after light irradiation, compared to treatment with light irradiation alone or **4** alone (Fig. 7 and S4†). The data demonstrates that photoactivation of **4** increases the percentage of cells displaying an increased ROS level by more than 27-fold compared with the treatment of **4** in the dark, leading to the observed photocytotoxicity. The increased ROS levels following light irradiation demonstrate, despite the lack of detection of $^1O_2$ in the Φ_Δ measurements, that **4** produces ROS species other than $^1O_2$ to induce photocytotoxicity.

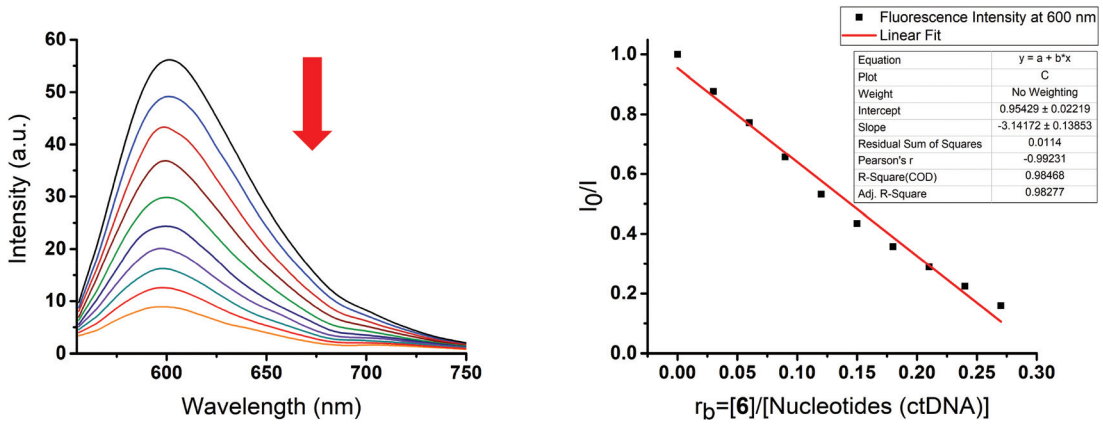

Fig. 6 Observed change in the fluorescence emission spectrum and at 600 nm of ctDNA bound EB with increasing concentration of **4**.

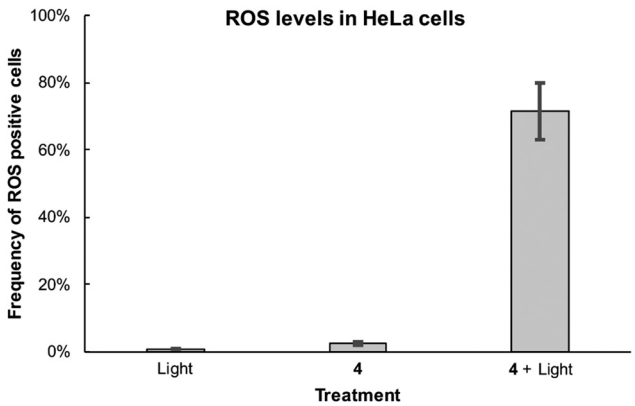

Fig. 7 Intracellular ROS levels in HeLa cells treated with 12 μM compound **4** for 4 h, irradiated with red light for 20 min. The ROS signal is indicated as DCF fluorescence, measured using the BL1 channel (excitation 488 nm, emission 530 nm) on an Attune NxT Cytometer and is plotted against side scatter (SSC). The results are an average of three independent experiments and the error bars represent standard deviation.

n-Octanol/water distribution

The *n*-octanol/water system has been widely used as a measure of lipophilicity/hydrophilicity in modelling biological partition/distribution to evaluate the distribution of potential drug candidates *in vivo*.[39] The distribution of compounds **2** and **4** in an *n*-octanol/PBS (pH 7.4) system was determined using the *shake-flask method* and quantified using RP-UPLC-ESI-MS (Fig. S5†).[40] The results showed that **2** is strongly lipophilic, as the compound was not detected in the PBS phase and showed complete accumulation in the *n*-octanol phase. This is in line with the known aqueous solubility-based limitations of similar compounds such as zinc phthalocyanine.[41] Conversely, the tetraplatinated compound **4** only accumulated in the aqueous phase while not being detectable in the *n*-octanol phase. This shows that the platination-induced fourfold positively charged character enhances the hydrophilicity, rendering the compound usable in aqueous systems such as the human body. Additionally, the high hydrophilicity of **4** is advantageous for fast renal clearance and to overcome issues connected with prolonged photosensitivity after treatment.[13]

Experimental

The chemicals used were obtained from Acros Organics, Chempur, Fluorochem, Fluka and Sigma-Aldrich, solvents used for analysis were of reaction grade (Emsure), the remaining solvents were of technical grade (Honeywell). Reactions were monitored for completion by analysing a small sample by TLC. Thin layer chromatography (TLC): Merck TLC plates silica gel 60 on aluminium with the indicated solvent system; the spots were visualized by UV light (254 nm and 366 nm). UV-Vis spectra: Specord® 250 PLUS spectrophotometer (Analytic Jena); λ_{max} in nm. Fluorescence emission spectra: FLS900 fluorescence spectrometer (Edinburgh Instruments); λ_{max} in nm. Fluorescence emission lifetime measurements were carried out on a FLS900 fluorescence spectrometer (Edinburgh Instruments) using an EPL-Laser (picosecond pulsed diode laser) for excitation and a cooled micro-channel plate photomultiplier (MCP-PMT) for single photon counting. Fluorescence quantum yields (Φ_f) were determined on a FLS900 fluorescence spectrometer (Edinburgh Instruments) using a F-M01 Integrating Sphere Assembly (Edinburgh Instruments) and the corresponding software (Edinburgh Instruments). Samples were measured as solutions in 1 cm quartz cells. IR spectra: SpectrumTwo FT-IR Spectrometer (PerkinElmer) equipped with a Specac Golden Gate™ ATR (attenuated total reflection) accessory; applied as neat samples; $1/\lambda$ in cm^{-1}. ^{195}Pt-NMR spectra in the indicated solvent mixture; Bruker AV-500 (107.5 MHz); δ in ppm rel. to K_2PtCl_6 in D_2O (δ 0). High-resolution electrospray mass spectra (HR-ESI-MS) were recorded on a maXis QTOF-MS instrument (Bruker). Samples were dissolved in an appropriate solvent at a concentration of around 1 μmol mL^{-1} and analyzed *via* continuous flow injection (2 μL min^{-1}). The mass spectrometer

was operated in the positive electrospray ionization mode at 4000 V capillary voltage, −500 V endplate offset, with a N_2 nebulizer pressure of 0.8 bar and dry gas flow of 4 l min^{-1} at 180 °C. Mass spectra were acquired in the mass range from m/z 50 to 2000 at 20 000 resolution (full width at half maximum) and 1.0 Hz rate. The mass analyzer was calibrated between m/z 118 and 2721 using an Agilent ESI-L low concentration tuning mix solution (Agilent) at a resolution of 20 000 and a mass accuracy below 2 ppm. All solvent used were purchased in best LC-MS qualities. Elemental analysis was performed on a LECO Truespec CHNS(O)-microanalyser. RP-UPLC-ESI-MS spectra of the compounds were measured on an Acquity Waters UPLC system coupled to Bruker HCT™ (Bremen) for the MS measurements, equipped with a DAD detector and an auto sampler using an Acquity UPLC BEH C18 analytical column (1.7 μm, 50 × 2.1 mm). The LC run (flow rate: 0.6 mL min^{-1}) was performed with a linear gradient of solvent A (distilled H_2O containing 0.1% v/v formic acid) and solvent B (CH_3CN (Sigma-Aldrich HPLC-grade)); t = 0–0.5 min, 5% B; t = 0.51–4 min, from 95% A (5% B) to 0% A (100% B); t = 4–5 min, 0% A, 100% B. UV-Vis detection was collected at 388 nm and 402 nm. Light irradiation experiments (except for the singlet oxygen quantum yield (Φ_Δ) determination) were performed using a Reflecta Diamator AF 2006 IR Hobby Line 250 W projector with a 600 nm long pass filter (square of 60 mm and 1 mm thick, Fig. S6†).

Synthetic procedures

Synthesis of tetra(3,4-pyrido)porphyrazine-zinc(II) (2).[25–27] A 100 mL two-necked round bottom flask, connected to a reflux condenser, was charged with *n*-pentanol (7.5 mL), $Zn(OAc)_2{\cdot}2H_2O$ (92.2 mg, 0.42 mmol) and 3,4-pyridinedicarbonitrile (**1**, 200 mg, 1.55 mmol). The mixture was stirred under a N_2 atmosphere at 100 °C for 10 min, afterwards DBU (0.23 ml, 1.55 mmol) was added dropwise and the mixture was stirred at 160 °C for 18 h. After completion of the reaction, the mixture was cooled to 23 °C and cyclohexane (40 mL) was added, then the mixture was kept at 23 °C for 2 h. The formed precipitate was filtered and washed with H_2O (20 mL) and hexane (20 mL) to afford a dark solid, which was further purified. The solid was dissolved in MeOH (20 mL) and stirred at 40 °C for 1 h before H_2O (30 mL) was added dropwise at 23 °C to precipitate the product, which was filtered and recovered with MeOH (20 mL). Finally, **2** was obtained as a dark blue solid (150 mg, 0.03 mmol, 64%) upon drying *in vacuo*.

Spectroscopic data of **2**: IR (Golden-Gate, [cm^{-1}]): 1663w (C═N), 1598m (C═C), 1571m, 1483m, 1428w, 1389m, 1336w, 1246m, 1189w, 1156w, 1073s, 1013s, 946w, 885m, 832m, 785w, 751m, 739s, 656w. UV-Vis (DMF, [nm], (log(ε [M^{-1} cm^{-1}]))): λ_{max} 388 (4.6), 603 (4.3), 663 (4.9), 674 (4.9). Fluorescence emission (DMF, [nm]): λ_{max} 680 (λ_{ex} 640). (+)-ESI-MS: 581 (100, $[M + H]^+$). Anal. calc. for $C_{28}H_{12}N_{12}Zn{\cdot}H_2O{\cdot}MeOH$ (631.91): C 55.12, H 2.87, N 26.60; found: C 54.76, H 2.28, N 26.36.

Synthesis of 29*H*,31*H*-tetra(3,4-pyrido)porphyrazine (3).[28] A 50 mL two-necked round bottom flask, connected to a reflux condenser, was charged with *n*-octanol (16 mL) and 3,4-pyridinedicarbonitrile (**1**, 300 mg, 2.33 mmol). The mixture was stirred at 100 °C for 10 min, afterwards DBU (1.40 mL, 9.32 mmol) was added dropwise and the mixture was heated to 185 °C for 40 min with stirring. The reaction mixture was then stirred at 185 °C for 2 h. After completion of the reaction, the mixture was cooled to 23 °C and the formed precipitate was filtered to afford a dark solid, which was further purified. The solid was dissolved in H_2O (30 mL) and stirred at 55 °C for 1 h. Afterwards the mixture was cooled down to 23 °C and the solvent was pipetted out before the solid was dried *in vacuo*. This purification procedure was repeated with MeOH (70 mL), acetone (70 mL) and cyclohexane (70 mL). Finally, **3** was obtained as a dark violet solid (88 mg, 0.02 mmol, 28%) by transferring of the solid with the aid of MeOH (20 mL) and drying *in vacuo*.

Spectroscopic data of **3**: IR (Golden-Gate, [cm^{-1}]): 1599m (C═C), 1498w, 1447w, 1412w, 1386w, 1323w, 1252w, 1237w, 1194w, 1156w, 1111m, 1077m, 1055w, 998s, 931w, 890w, 874m, 831m, 744s, 736s, 687m. UV-Vis (DMF, [nm], (log(ε [M^{-1} cm^{-1}]))): λ_{max} 380 (4.5), 607 (4.3), 660 (4.7), 669 (4.7). Fluorescence emission (DMF, [nm]): λ_{max} 678 (λ_{ex} 640). (+)-ESI-MS: 519 (100, $[M + H]^+$). Anal. calc. for $C_{28}H_{14}N_{12}{\cdot}H_2O{\cdot}MeOH$ (568.54): C 61.26, H 3.55, N 29.56; found: C 61.79, H 2.94, N 29.18.

Synthesis of [tetrakis-(*trans*-Pt(NH_3)$_2$Cl)-tetra(3,4-pyrido)porphyrazine-zinc(II)](NO_3)$_4$ (4). A 20 mL round bottom flask was charged with DMF (2 mL), *trans*-Pt(NH_3)$_2Cl_2$ (**6**, 45 mg, 0.15 mmol) and $AgNO_3$ (26 mg, 0.15 mmol). The mixture was stirred at 55 °C for 23 h under exclusion of light, afterwards the mixture was centrifuged and the yellow solution was transferred into a 20 mL round bottom flask. A solution of tetra(3,4-pyrido)porphyrazine-zinc(II) (**2**) (20 mg, 0.03 mmol) in DMF (2 mL) was added and the mixture was stirred at 50 °C for 48 h with exclusion of light. After completion of the reaction, the mixture was cooled to 23 °C and MTBE (5 mL) was added. The mixture was filtered after 15 min, yielding a dark green precipitate. The precipitate was washed with MeOH, DCM, MTBE and *n*-hexane. Finally, **4** was obtained as a dark green solid (31 mg, 0.02 mmol, 48%) by transferring the solid with the aid of *n*-hexane (10 mL) and drying *in vacuo*.

Spectroscopic data of **4**: IR (Golden-Gate, [cm^{-1}]): 3096w, 1622m, 1489m, 1312s, 1157w, 1083s, 911s, 823m, 848m, 761s, 744s, 688m, 668m. UV-Vis (DMF, [nm], (log(ε [M^{-1} cm^{-1}]))): λ_{max} 402 (4.6), 680 (5.0), 691 (5.0). Fluorescence emission (DMF, [nm]): λ_{max} 678 (λ_{ex} 640). ^{195}Pt-NMR (DMSO-d_6 : methanol-d_4 = 9 : 1): −3136 (s, 4 × Pt, Fig. S1†). (+)-ESI-MS (DMF): 881 (4, $[M - 2NO_3]^{2+}$), 855 (3, $[M + Cl - 3NO_3]^{2+}$), 567 (30, $[M - 3NO_3]^{3+}$), 558 (60, $[M + Cl - 4NO_3]^{3+}$), 410 (30, $[M - 4NO_3]^{4+}$). Anal. calc. for $C_{28}H_{36}Cl_4N_{24}O_{12}Pt_4Zn{\cdot}0.5$ *n*-hexane (1931.36): C 19.28, H 2.24, N 17.41; found: C 19.40, H 2.36, N 17.36.

Singlet oxygen quantum yields. The singlet oxygen quantum yields (Φ_Δ) of **2**, **3** and **4** were determined analogously to a method reported by Bonnet and coworkers.[42] The PSs were dissolved in DMF-d_7 and the solutions were placed in a glass cuvette (114F-10-40, 10 mm × 4 mm dimensions, Hellma

Analytics). The concentrations were adjusted to an absorption intensity of 0.13 ± 0.02 at 630 nm, with the cuvette oriented in a way that the light path equals to 10 mm. The cuvettes containing the samples were placed in a CUV-UV/VIS-TC-ABS temperature-controlled Qpod sample compartment (Avantes) and cooled to 20 °C; temperature control was performed with the use of a TC-125 controller (Quantum Northwest) and Q-Blue software. Emission spectroscopy was conducted in a custom-built setup (Fig. S7†), that is based on the setup described by Meijer *et al.*[42] Excitation was performed using a high-power-LED 630 nm light source (FC5-LED-WL, Prismatix). The light source was connected with an optical fibre (1000 μm core diameter, Avantes) to the cuvette holder over a SMA 905 fibre optic connector. The intensity of the light source was measured to be 10.0 mW cm^{-2} at the position of the cuvette. The excitation power was measured using a S310C thermal sensor connected to a PM100USB power meter (Thorlabs). The connection piece used to insert the SMA connector into the cuvette holder was replaced by an in-house custom-built connection piece that allows the fibre to be inserted at a distance of 2.0 cm from the cuvette. The detector (AvaSpec-NIR256-1.7TEC, Avantes) was set to 0 °C and connected to the cuvette holder with an optical fibre (600 μm diameter, Avantes). Emission spectra were collected at a 90° angle with respect to the excitation beam from 1100 to 1400 nm after three measurement runs; every measurement run consisted of five averaged measurements each lasting 9 s. All spectra were recorded using AvaSoft 8.9 software from Avantes and further processed using Microsoft Office Excel and Origin 2018 software.

The singlet oxygen quantum yields were calculated by comparison with a known literature standard (zinc phthalocyanine (ZnPc): $\Phi_\Delta = 0.56$ in DMF),[43] according to eqn (E2).

$$\Phi_{\Delta(x)} = \Phi_{\Delta(\mathrm{std})}\left(\frac{I^{630}_{\mathrm{std}}}{I^{630}_{\mathrm{x}}}\right)\left(\frac{E_{\mathrm{x}}}{E_{\mathrm{std}}}\right) \quad \text{(E2)}$$

In (E2), the subscript × designates the corresponding photosensitizer and std the standard (ZnPc). Φ_Δ is the singlet oxygen quantum yield. I^{630} is the rate of light absorption calculated as overlap of the absorption spectrum of either PS or standard and the emission spectrum of the LED light source at 630 nm. E is the integrated emission peak of singlet oxygen at around 1270 nm. For these emission spectra, the integrated values were obtained by applying a manual background correction in Origin (Fig. S8†).

Cell culture. Human cervical carcinoma cells (HeLa) were cultured in DMEM (Gibco) supplemented with 5% fetal calf serum (Gibco), 100 U mL^{-1} penicillin, 100 μg mL^{-1} streptomycin. The cells were grown at 37 °C and in 5% CO_2 humidified atmosphere.

Photocytotoxicity assays. The PS toxicity under light and dark conditions was evaluated for a HeLa cell line, using a resazurin-based fluorometric cell viability assay. Stock solutions of the PS (3 mg mL^{-1}) were prepared in DMF and stored in the dark. The respective stock solutions were further diluted with the complete medium to desired working concentrations. For a typical experiment, 100 μL aliquots of cells in growth medium were seeded in 96-well plates (density of 4×10^3 cells per well) and incubated at 37 °C and 5% CO_2. After 24 h of incubation, cells were treated with different concentrations (32 nM–100 μM, 200 μL final well volume) of the test compounds and incubated for 4 h under light exclusion. For light irradiation experiments, cells were treated for 4 h with compounds, and the medium was replaced by fresh medium. Each sample was placed 3 cm away from the red cut-off filter from the projector. Cells were exposed to light (white light projector with 600 nm filter) for 20 min (light intensity: 5.8 mW cm^{-2} for 20 min, light dose: 6.96 J cm^{-2}), followed by additional incubation for 20 h. Thereafter, for all experiments, the medium was removed, 100 μL of freshly prepared resazurin containing complete medium (0.2 mg mL^{-1} final concentration) was added, and cells were incubated at 37 °C for 4 h. Fluorescence of the resorufin product (λ_{ex} = 540 nm) was quantified at 590 nm using a SpectraMax M5 microplate Reader. The reported cytotoxicity is an average of at least two independent experiments, with triplicate determinations for each drug concentration and the error bars demarcate the standard deviation (S.D.). Final DMF concentration in the wells was less than 0.5% (v/v) and control experiments with the same amount of DMF in culture medium showed no cytotoxic effect (results not shown).

Localization studies. HeLa cells were seeded in Ibidi μ-Slide 8-well glass bottom dishes and allowed to reach ≈70% confluency. The medium was replaced with new medium and freshly prepared solutions of drugs with a final concentration of 50 μM were added. After 2 h incubation with compounds, the cells were washed three times with PBS (0.5 mL) and stored in fresh media containing 10% FBS for live-cell imaging. Prior to imaging, the cells were incubated for 5 min with 1.5 μM Hoechst 33258 (final concentrations). The fluorescence of **4** was visualized with excitation from a 633 nm HeNe laser and the red emission was collected using a 650 nm long pass filter.

Detection of intracellular ROS levels. 2×10^5 HeLa cells in 2 mL DMEM supplemented with 5% FBS were seeded on 60 mm dishes. The following day, cells were treated with 12 μM compound **4** for 4 hours. Following the incubation, cells were washed with PBS and the medium was subsequently replaced with 2 mL DMEM. Cells were irradiated for 20 min with red light, as described for the photocytotoxicity assays. After irradiation, H_2DCF-DA was added to the samples to a final concentration of 50 μM and incubated for 30 minutes at 37 °C. Cells were washed twice with PBS and collected by trypsinisation. Cells were suspended in 1 mL PBS containing 1% FBS. Samples were analysed on an Attune NxT Cytometer (Thermo Fisher Scientific) using BL1 channel (excitation 488 nm, emission 515 nm) to measure DCF fluorescence. Results are expressed as mean percentage of ROS levels over cell population, obtained from three independent experiments with a minimum of 100 000 cells analysed per condition. The error bars represent standard deviation (S.D).

Determination of the *n*-octanol/water distribution. Stock solutions (10 mM) of compounds **2** and **4** were prepared in DMSO and diluted with a PBS (pH 7.4)/*n*-octanol system (1 : 1) to reach a final compound concentration of 2.5 mM in a volume of 1 mL. The mixtures were subsequently vortexed before equilibration at 23 °C during 24 h. Then, the phases were separated and diluted equally (PBS phase in H_2O, *n*-octanol phase in MeOH) to reach UPLC-suitable concentrations. The relative concentration of each compound in the *n*-octanol and PBS phase was determined through the area under curve in the analytical UPLC spectra.

Conclusion

The first exocyclically metallated tetrapyridinoporphyrazine **4** was synthesized, characterized and its photochemical and photophysical properties as well as its phototoxicity against a human cancer HeLa cell line were determined. A comparison of the IC_{50} values of **4** and its nonplatinated precursor **2** shows a clear improved effectivity of the substance emerging through the exocyclic platination. Besides the additional heavy atom effect emerging through the platinum species coupled to the photochemical system, the platinum complexes help to increase the solubility of tetrapyridinoporphyrazine PS in aqueous media, induce a dual chemotherapeutic effect and potentially increase the cellular uptake. We therefore propose the further investigation of platinum(II)-coupled PS for PDT.

Conflicts of interest

There are no conflicts of interest to declare.

Acknowledgements

We thank the University of Zürich and the Swiss National Science Foundation (205321_159976) for financial support. WW is supported by a Swiss Government Excellence Scholarship and the Novartis Foundation for Medical-Biological Research. SF is supported by the Czech Science Foundation grant 17-02080S. We thank Mathias Mosberger for the help with the fluorescence lifetime measurements, Dr Thomas Fox for recording the ^{195}Pt-NMR spectrum and Dr Michael S. Meijer as well as Prof. Sylvestre Bonnet for many helpful discussions concerning singlet oxygen quantum yield determination. Imaging was performed with equipment maintained by the Center for Microscopy and Image Analysis, University of Zurich.

References

1 L. M. Moreira, F. V. dos Santos, J. P. Lyon, M. Maftoum-Costa, C. Pacheco-Soares and N. S. da Silva, Photodynamic therapy: Porphyrins and phthalocyanines as Photosensitizers, *Aust. J. Chem.*, 2008, **61**, 741–754.

2 I. Yoon, J. Z. Li and Y. K. Shim, Advance in photosensitizers and light delivery for photodynamic therapy, *Clin. Endosc.*, 2013, **46**, 7–23.

3 Z. Jiang, J. Shao, T. Yang, J. Wang and L. Jia, Pharmaceutical development, composition and quantitative analysis of phthalocyanine as the photosensitizer for cancer photodynamic therapy, *J. Pharm. Biomed. Anal.*, 2014, **87**, 98–104.

4 Y. Li, J. Wang, X. Zhang, W. Guo, F. Li, M. Yu, X. Kong, W. Wu and Z. Hong, Highly water-soluble and tumor-targeted photosensitizers for photodynamic therapy, *Org. Biomol. Chem.*, 2015, **13**, 7681–7694.

5 P. M. Antoni, A. Naik, I. Albert, R. Rubbiani, S. Gupta, P. Ruiz-Sanchez, P. Munikorn, J. M. Mateos, V. Luginbuehl, P. Thamyongkit, U. Ziegler, G. Gasser, G. Jeschke and B. Spingler, (Metallo)porphyrins as Potent Phototoxic Anti-Cancer Agents after Irradiation with Red Light, *Chem. – Eur. J.*, 2015, **21**, 1179–1183.

6 J. M. Dabrowski, B. Pucelik, A. Regiel-Futyra, M. Brindell, O. Mazuryk, A. Kyziol, G. Stochel, W. Macyk and L. G. Arnaut, Engineering of relevant photodynamic processes through structural modifications of metallotetrapyrrolic photosensitizers, *Coord. Chem. Rev.*, 2016, **325**, 67–101.

7 D. van Straten, V. Mashayekhi, H. S. de Bruijn, S. Oliveira and D. J. Robinson, Oncologic Photodynamic Therapy: Basic Principles, Current Clinical Status and Future Directions, *Cancers*, 2017, **9**, 19.

8 J. Zhang, C. Jiang, J. P. Figueiró Longo, R. B. Azevedo, H. Zhang and L. A. Muehlmann, An updated overview on the development of new photosensitizers for anticancer photodynamic therapy, *Acta Pharm. Sin. B*, 2018, **8**, 137–146.

9 S. G. Bown, Photodynamic therapy for photochemists, *Philos. Trans. R. Soc., A*, 2013, **371**, 20120371.

10 K. Ishii, Functional singlet oxygen generators based on phthalocyanines, *Coord. Chem. Rev.*, 2012, **256**, 1556–1568.

11 H. Abrahamse and M. R. Hamblin, New photosensitizers for photodynamic therapy, *Biochem. J.*, 2016, **473**, 347–364.

12 J.-Y. Liu, X.-J. Jiang, W.-P. Fong and D. K. P. Ng, Highly photocytotoxic 1,4-dipegylated zinc(II) phthalocyanines. Effects of the chain length on the *in vitro* photodynamic activities, *Org. Biomol. Chem.*, 2008, **6**, 4560–4566.

13 D. E. J. G. J. Dolmans, D. Fukumura and R. K. Jain, Photodynamic therapy for cancer, *Nat. Rev. Cancer*, 2003, **3**, 380–387.

14 A. Naik, R. Rubbiani, G. Gasser and B. Spingler, Visible-Light-Induced Annihilation of Tumor Cells with Platinum–Porphyrin Conjugates, *Angew. Chem., Int. Ed.*, 2014, **53**, 6938–6941.

15 A. Oniszczuk, K. A. Wojtunik-Kuleszaa, T. Oniszczuk and K. Kasprzak, The potential of photodynamic therapy (PDT)-Experimental investigations and clinical use, *Biomed. Pharmacother.*, 2016, **83**, 912–929.

16 L. Hassani, F. Hakimian, E. Safaei and Z. Fazeli, Antibacterial effect of cationic porphyrazines and anionic phthalocyanine and their interaction with plasmid DNA, *J. Mol. Struct.*, 2013, **1052**, 221–227.
17 M. Machacek, J. Demuth, P. Cermak, M. Vavreckova, L. Hruba, A. Jedlickova, P. Kubat, T. Simunek, V. Novakova and P. Zimcik, Tetra(3,4-pyrido)porphyrazines Caught in the Cationic Cage: Toward Nanomolar Active Photosensitizers, *J. Med. Chem.*, 2016, **59**, 9443–9456.
18 M. P. Donzello, E. Viola, X. Cai, L. Mannina, C. Ercolani and K. M. Kadish, Tetra-2,3-pyrazinoporphyrazines with Externally Appended Pyridine Rings. 8. Central (Zn^{II}, Cu^{II}, $Mg^{II}(H_2O)$, Cd^{II}) and Exocyclic (Pd^{II}) Metal Ion Binding in Heteropentametallic Complexes from Tetrakis-2,3-[5,6-di(2-pyridyl)pyrazino]porphyrazine, *Inorg. Chem.*, 2010, **49**, 2447–2456.
19 I. Manet, F. Manoli, M. P. Donzello, E. Viola, A. Masi, G. Andreano, G. Ricciardi, A. Rosa, L. Cellai, C. Ercolani and S. Monti, Pyrazinoporphyrazines with Externally Appended Pyridine Rings. 13. Structure, UV-Visible Spectral Features, and Noncovalent Interaction with DNA of a Positively Charged Binuclear (Zn^{II}/Pt^{II}) Macrocycle with Multimodal Anticancer Potentialities, *Inorg. Chem.*, 2013, **52**, 321–328.
20 M. P. Donzello, D. Vittori, D. Futur, Z. Fu, C. Ercolani and K. M. Kadish, Tetra-2,3-pyrazinoporphyrazines with externally appended pyridine rings. 14. UV-visible spectral and electrochemical behavior of homo/heterobinuclear neutral and hexacationic macrocycles, *J. Porphyrins Phthalocyanines*, 2013, **17**, 896–904.
21 M. P. Donzello, F. Gigante, F. Sciscione, E. Viola and K. M. Kadish, Tetra-2,3-pyrazinoporphyrazines with externally appended pyridine rings. 18. Physicochemical properties and photochemical behavior of new uncharged water soluble low-symmetry macrocycles [$\{Pd(OAc)_2\}_3(PtCl_2)$LM] (M = $Mg^{II}(H_2O)$, Zn^{II}, Pd^{II}), *J. Porphyrins Phthalocyanines*, 2017, **21**, 334–344.
22 A.-M. Florea and D. Büsselberg, Cisplatin as an Anti-Tumor Drug: Cellular Mechanisms of Activity, Drug Resistance and Induced Side Effects, *Cancers*, 2011, **3**, 1351–1371.
23 Y. Jung and S. J. Lippard, Direct cellular responses to platinum-induced DNA damage, *Chem. Rev.*, 2007, **107**, 1387–1407.
24 O. Vrana, V. Novohradsky, Z. Medrikova, J. Burdikova, O. Stuchlikova, J. Kasparkova and V. Brabec, Internalization of Ineffective Platinum Complex in Nanocapsules Renders It Cytotoxic, *Chem. – Eur. J.*, 2016, **22**, 2728–2735.
25 W. S. Szulbinski and J. R. Kincaid, Synthesis and spectroscopic characterization of zinc tetra(3,4-pyridine)porphyrazine entrapped within the supercages of Y-zeolite, *Inorg. Chem.*, 1998, **37**, 5014–5020.
26 C. Martí, S. Nonell, M. Nicolau and T. Torres, Photophysical properties of neutral and cationic tetrapyridinoporphyrazines, *Photochem. Photobiol.*, 2000, **71**, 53–59.
27 E. A. Dupouy, D. Lazzeri and E. N. Durantini, Photodynamic activity of cationic and non-charged Zn(II) tetrapyridinoporphyrazine derivatives: biological consequences in human erythrocytes and Escherichia coli, *Photochem. Photobiol. Sci.*, 2004, **3**, 992–998.
28 C. Ramirez, C. Antonacci, J. Ferreira and R. D. Sheardy, The facile synthesis and characterization of novel cationic metallated and nonmetallated tetrapyridino porphyrazines having different metal centers, *Synth. Commun.*, 2004, **34**, 3373–3379.
29 H. Tomoda, S. Saito, S. Ogawa and S. Shiraishi, Synthesis of Phthalocyanines from Phthalonitrile with Organic Strong Bases, *Chem. Lett.*, 1980, **9**, 1277–1280.
30 M. Obata, S. Hirohara, R. Tanaka, I. Kinoshita, K. Ohkubo, S. Fukuzumi, M. Tanihara and S. Yano, In Vitro Heavy-Atom Effect of Palladium(II) and Platinum(II) Complexes of Pyrrolidine-Fused Chlorin in Photodynamic Therapy, *J. Med. Chem.*, 2009, **52**, 2747–2753.
31 S. Fukuzumi, K. Ohkubo, X. Zheng, Y. Chen, R. K. Pandey, R. Zhan and K. M. Kadish, Metal Bacteriochlorins Which Act as Dual Singlet Oxygen and Superoxide Generators, *J. Phys. Chem. B*, 2008, **112**, 2738–2746.
32 M. Bregnhøj, M. Westberg, F. Jensen and P. R. Ogilby, Solvent-dependent singlet oxygen lifetimes: temperature effects implicate tunneling and charge-transfer interactions, *Phys. Chem. Chem. Phys.*, 2016, **18**, 22946–22961.
33 L. Vachova, M. Machacek, R. Kucera, J. Demuth, P. Cermak, K. Kopecky, M. Miletin, A. Jedlickova, T. Simunek, V. Novakova and P. Zimcik, Heteroatom-substituted tetra(3,4-pyrido)porphyrazines: a stride toward near-infrared-absorbing macrocycles, *Org. Biomol. Chem.*, 2015, **13**, 5608–5612.
34 J. Piskorz, K. Konopka, N. Düzgünes, Z. Gdaniec, J. Mielcarek and T. Goslinski, Diazepinoporphyrazines Containing Peripheral Styryl Substituents and Their Promising Nanomolar Photodynamic Activity against Oral Cancer Cells in Liposomal Formulations, *ChemMedChem*, 2014, **9**, 1775–1782.
35 P. Skupin-Mrugalska, W. Szczolko, P. Gierlich, K. Konopka, T. Goslinski, J. Mielcarek and N. Düzgünes, Physicochemical properties of liposome-incorporated 2-(morpholin-4-yl)ethoxy phthalocyanines and their photodynamic activity against oral cancer cells, *J. Photochem. Photobiol., A*, 2018, **353**, 445–457.
36 N. Y. Shilyagina, N. N. Peskova, S. A. Lermontova, A. A. Brilkina, V. A. Vodeneev, A. V. Yakimansky, L. G. Klapshina and I. V. Balalaeva, Effective delivery of porphyrazine photosensitizers to cancer cells by polymer brush nanocontainers, *J. Biophotonics*, 2017, **10**, 1189–1197.
37 D. L. Boger, B. E. Fink, S. R. Brunette, W. C. Tse and M. P. Hedrick, A simple, high-resolution method for establishing DNA binding affinity and sequence selectivity, *J. Am. Chem. Soc.*, 2001, **123**, 5878–5891.
38 R. P. Rastogi, S. P. Singh, D.-P. Häder and R. P. Sinha, Detection of reactive oxygen species (ROS) by the oxidant-sensing probe 2′,7′-dichlorodihydrofluorescein diacetate in the cyanobacterium Anabaena variabilis PCC 7937, *Biochem. Biophys. Res. Commun.*, 2010, **397**, 603–607.

39 S. S. Bharate, V. Kumar and R. A. Vishwakarma, Determining Partition Coefficient (Log P), Distribution Coefficient (Log D) and Ionization Constant (pKa) in Early Drug Discovery, *Comb. Chem. High Throughput Screening*, 2016, **19**, 461–469.

40 V. Pierroz, T. Joshi, A. Leonidova, C. Mari, J. Schur, I. Ott, L. Spiccia, S. Ferrari and G. Gasser, Molecular and Cellular Characterization of the Biological Effects of Ruthenium(II) Complexes Incorporating 2-Pyridyl-2-pyrimidine-4-carboxylic Acid, *J. Am. Chem. Soc.*, 2012, **134**, 20376–20387.

41 H. K. Moon, M. Son, J. E. Park, S. M. Yoon, S. H. Lee and H. C. Choi, Significant increase in the water dispersibility of zinc phthalocyanine nanowires and applications in cancer phototherapy, *NPG Asia Mater.*, 2012, **4**, e12.

42 M. S. Meijer, V. S. Talens, M. F. Hilbers, R. E. Kieltyka, A. M. Brouwer, M. M. Natile and S. Bonnet, NIR-Light-Driven Generation of Reactive Oxygen Species Using Ru(II)-Decorated Lipid-Encapsulated Upconverting Nanoparticles, *Langmuir*, 2019, **35**, 12079–12090.

43 U. Michelsen, H. Kliesch, G. Schnurpfeil, A. K. Sobbi and D. Wöhrle, Unsymmetrically substituted benzonaphthoporphyrazines: A new class of cationic photosensitizers for the photodynamic therapy of cancer, *Photochem. Photobiol.*, 1996, **64**, 694–701.

Supporting Information for

Exocyclically Metallated Tetrapyridinoporphyrazine as a Potential Photosensitizer for Photodynamic Therapy

Lukas Schneider,[a] Michele Larocca,[a] Wenyu Wu,[a] Vipin Babu,[a] Roxane Padrutt,[a] Ekaterina Slyshkina,[a] Christiane König,[b] Stefano Ferrari,[b,c] Bernhard Spingler[a]

[a] Department of Chemistry, University of Zurich, Winterthurerstrasse 190, 8057 Zurich, Switzerland. E-mail: spingler@chem.uzh.ch; Web: http://www.chem.uzh.ch/en/research/spingler.html; Fax: +41 44 635 68 02; Tel: +41 44 635 46 56

[b] Institute of Molecular Cancer Research, University of Zurich, Winterthurerstrasse 190, 8057 Zurich, Switzerland. E-mail: sferrari@imcr.uzh.ch; Web: http://www.imcr.uzh.ch/research/Ferrari.html; Fax: +41 44 635 34 84; Tel: +41 44 635 34 71

[c] Institute of Molecular Genetics, Academy of Sciences of the Czech Republic, Videnska 1083, 143 00, Prague, Czech Republic

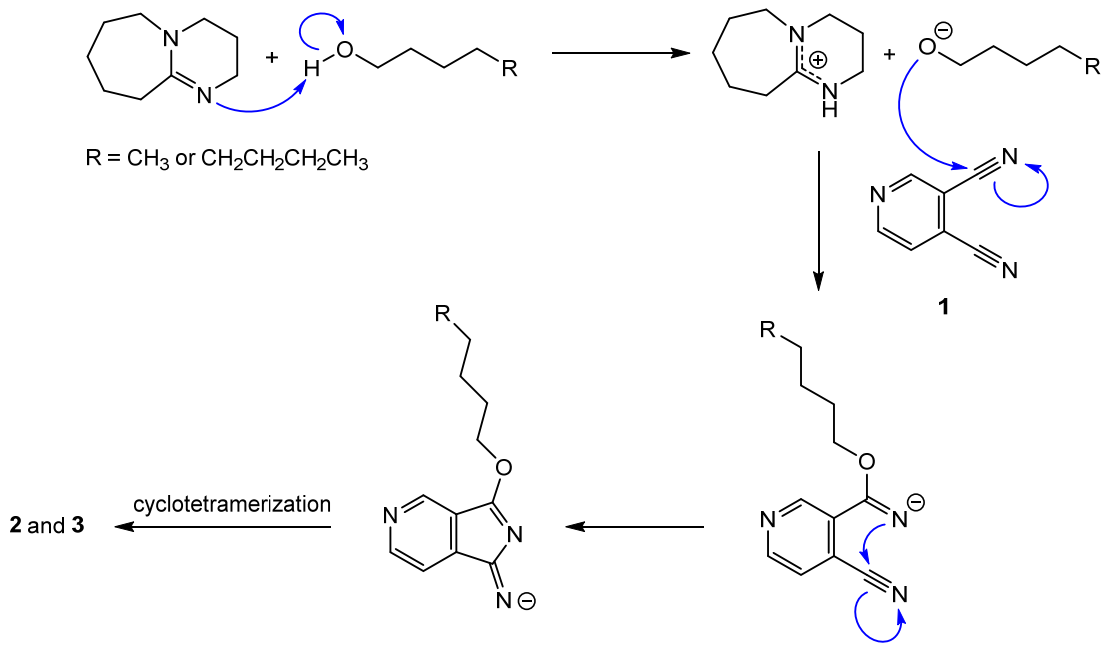

Scheme S1. A reaction mechanism for the formation of **2** and **3** analogous to the one proposed by Tomoda *et al.*[1]

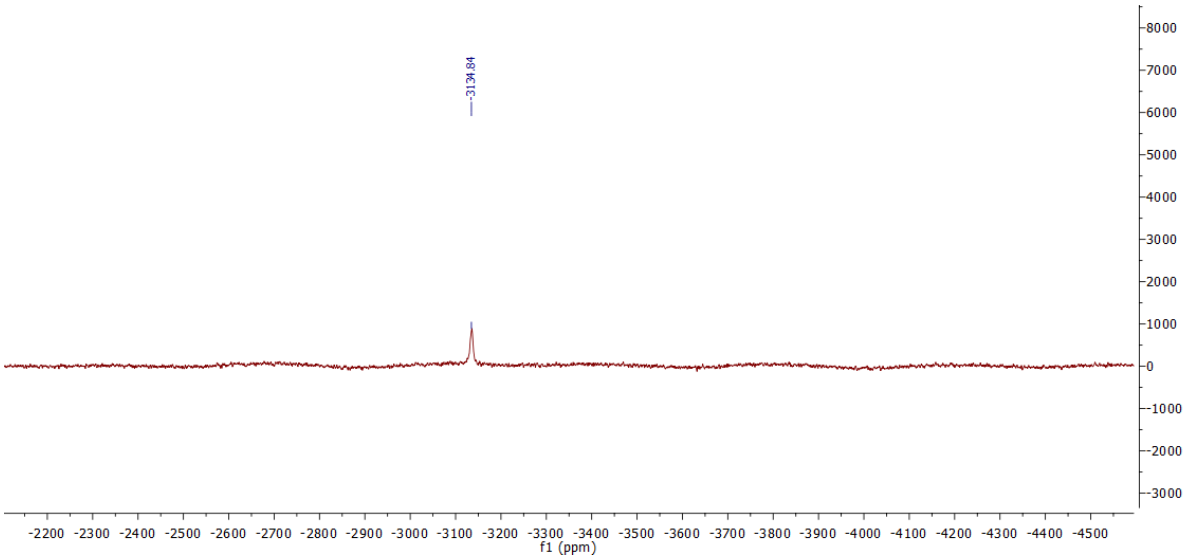

Figure S1: ^{195}Pt-NMR spectrum of **4** measured in DMSO-d_6:Methanol-d_4 = 9:1.

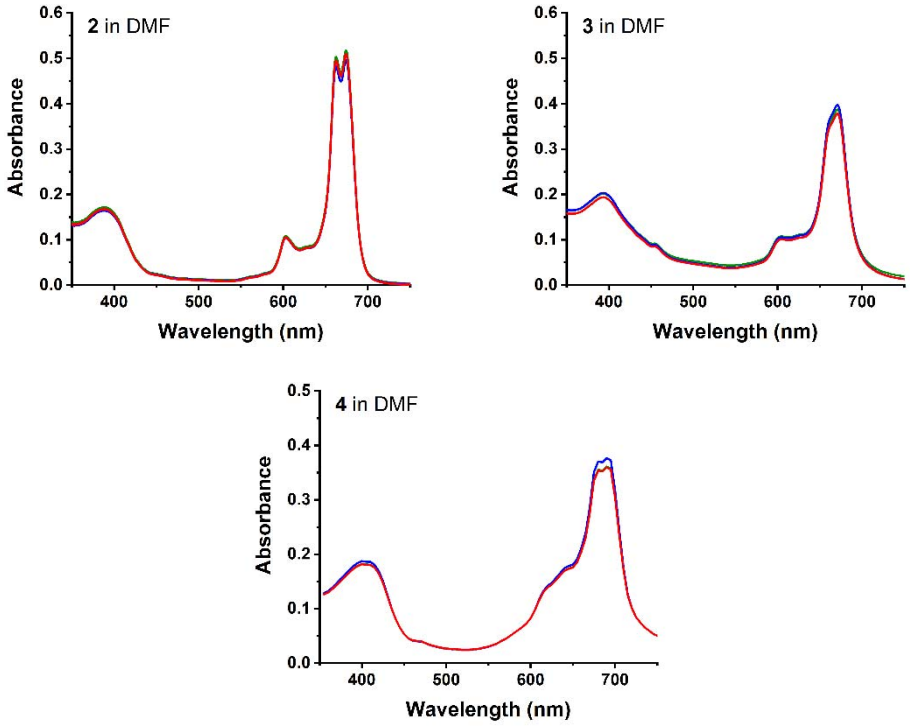

Figure S2. UV-Vis absorbance spectra of **2**, **3** and **4** in DMF: Instantly measured (green), after one week under light exclusion (blue) and after one additional week in daylight (red).

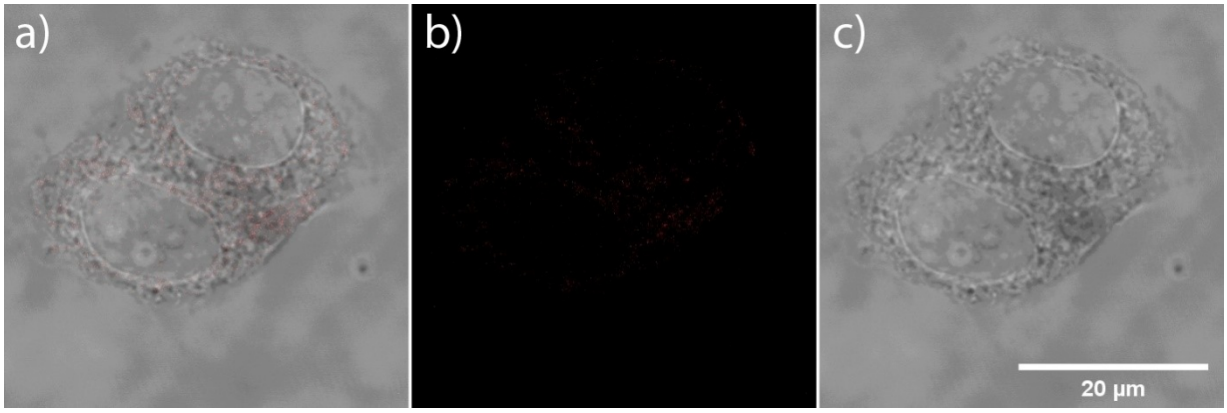

Figure S3. Control experiment for the intracellular localization of compound **4** in HeLa cells. Confocal images of cells without Hoechst 33258 staining and without compound **4** are shown: a) merge, b) red channel, c) white field.

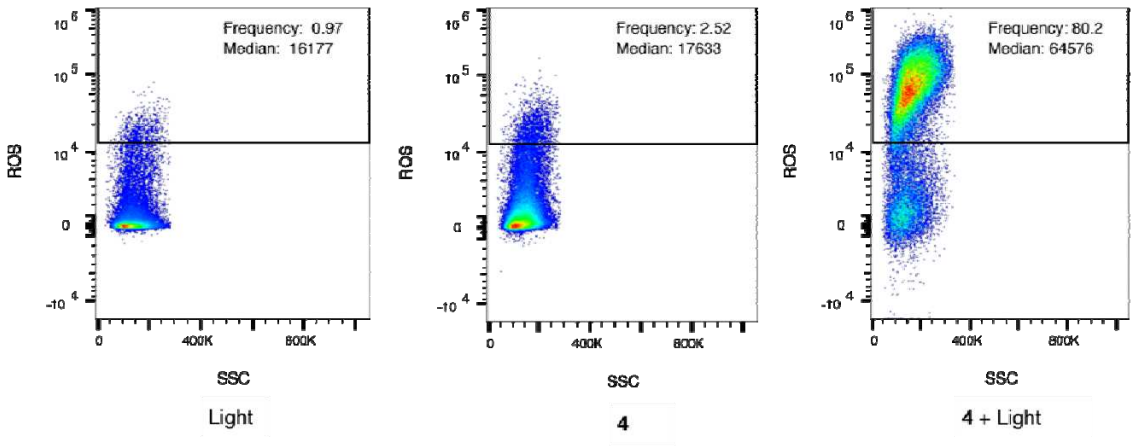

In the table below, the average ROS levels for 3 independent experiments are given.

Treatment	Frequency	S.D
Light	0.64	0.34
4	2.53	0.49
4 + Light	71.5	8.46

Figure S4. A typical experiment showing the intracellular ROS levels in HeLa cells irradiated with red light for 20 min (left), treated with 12 µM compound **4** for 4 h (middle) or treated with 12 µM compound **4** for 4 h and irradiated with red light for 20 min (right). ROS signal is indicated as DCF fluorescence, measured using the BL1 channel (excitation 488 nm, emission 530 nm) on an Attune NxT Cytometer and is plotted against side scatter (SSC). The median fluorescence intensity and the frequency of cells displaying ROS signal are shown. S.D designates the standard deviation.

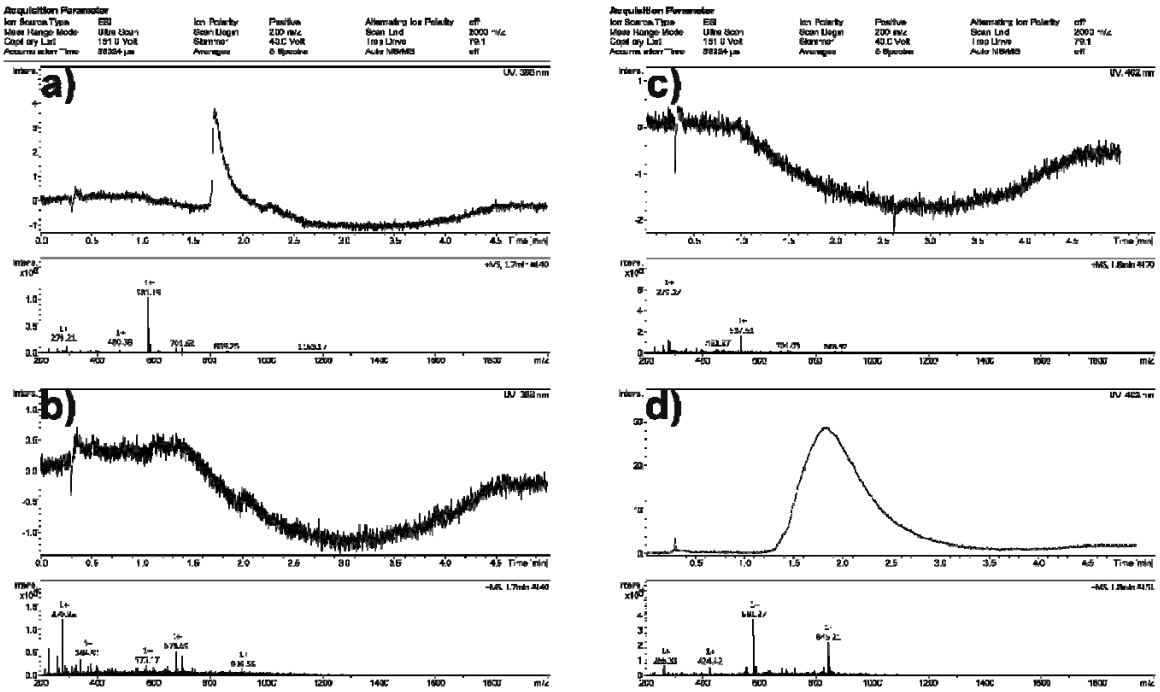

Figure S5. RP-UPLC-ESI-MS spectra of a) *n*-octanol phase (**2**), b) PBS phase (**2**), c) *n*-octanol phase (**4**), d) PBS phase (**4**), showing that **2** only accumulates in the *n*-octanol phase and **4** only in the PBS phase.

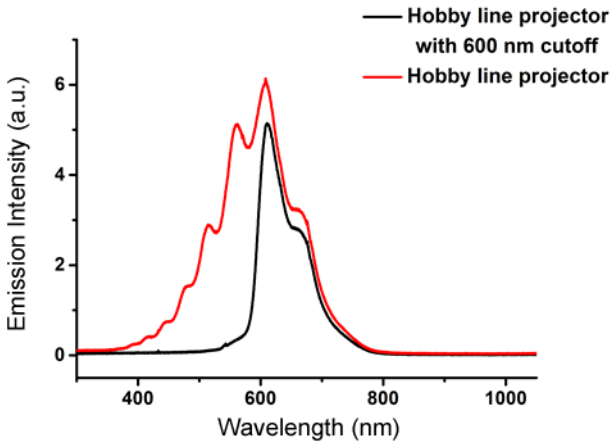

Figure S6. Emission of the white light projector with and without an applied filter at 600 nm.

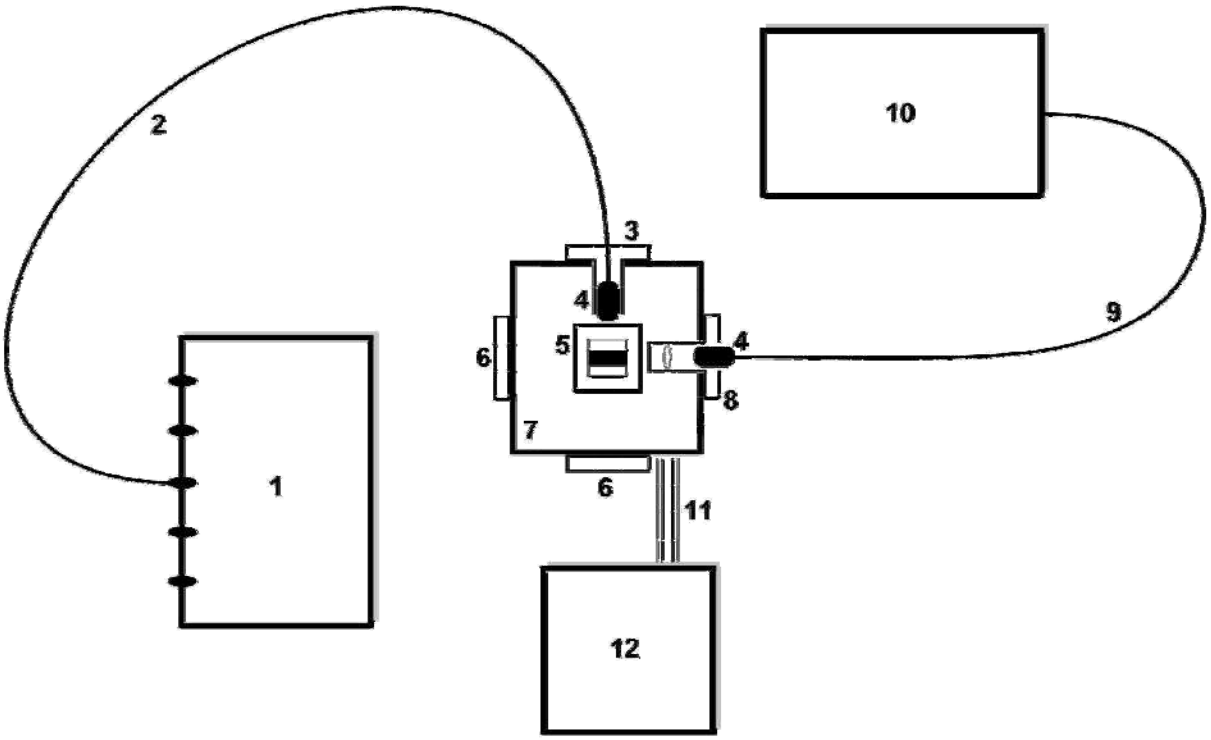

Figure S7. Setup used for NIR emission spectroscopy. **1)** LED light source, **2)** Optical fibre (1000 µm), **3)** Custom-built connection piece, **4)** SMA 905 fibre optic connector, **5)** Cuvette in cuvette holder, **6)** Blank, **7)** Temperature-controlled Qpod cuvette holder, **8)** Connection piece with QIL-UV AR-coated fused-silica imaging lens, **9)** Optical fibre (600 µm), **10)** NIR detector, **11)** Plastic hose, **12)** Cooling bath.

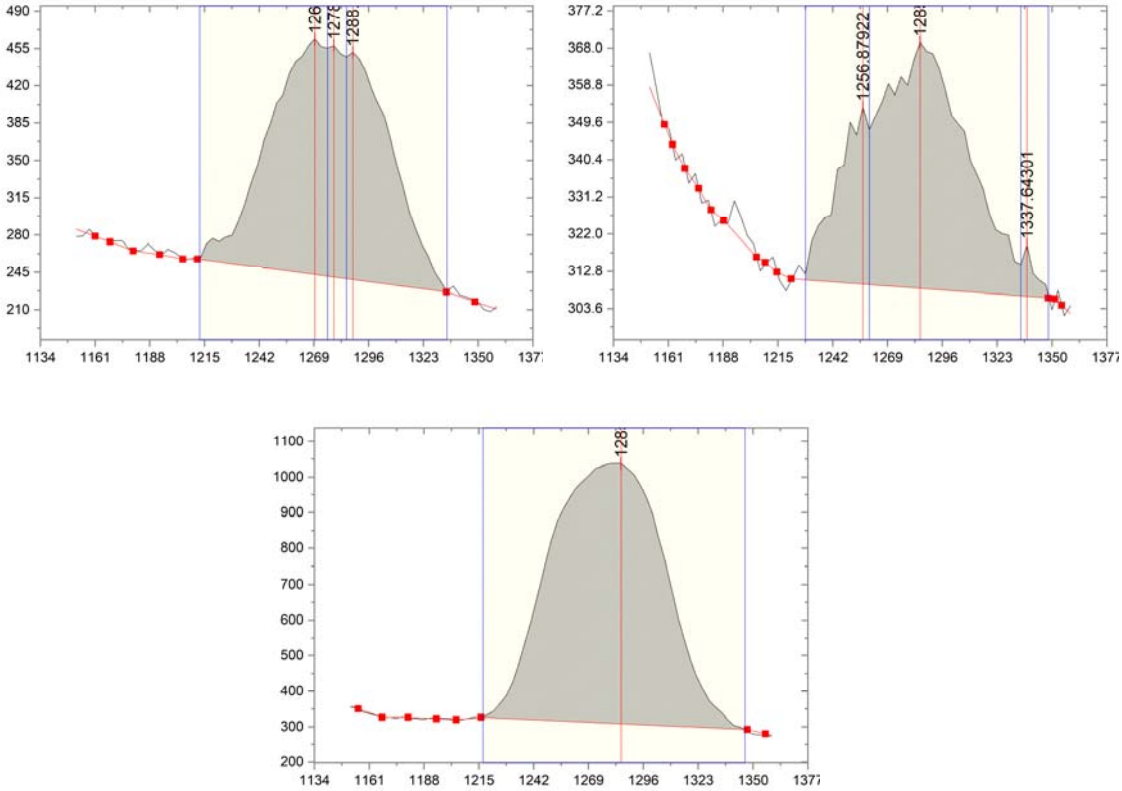

Figure S8. Singlet oxygen phosphorescence emission intensity (a.u.) vs. wavelength (nm) plots of the measured solutions of substances **2** (top left), **3** (top right), and zinc phthalocyanine (**ZnPc**, bottom left).

References

1. H. Tomoda, S. Saito, S. Ogawa and S. Shiraishi, Synthesis of Phthalocyanines from Phthalonitrile with Organic Strong Bases, *Chem. Lett.*, 1980, **9**, 1277-1280.